Using networked Pandora observations to capture spatiotemporal changes in total column ozone associated with stratosphere-to-troposphere transport

J. Robinson[1,2], A. Kotsakis[2,3], F. Santos[4,5], R. Swap[2,6], K. E. Knowland[2,3], G. Labow[2,7], V. Connors[8], M. Tzortziou[2,9], N. Abuhassan[1,2], M. Tiefengraber[10], and A. Cede[3,10]

[1]Joint Center for Earth Systems Technology, University of Maryland, Baltimore County, Baltimore, MD, USA, [2]NASA Goddard Space Flight Center, Greenbelt, MD, USA, [3]Universities Space Research Association/Goddard Earth Science Technology & Research, Columbia, MD, USA, [4]Earth System Science Interdisciplinary Center, University of Maryland, College Park, MD, USA, [5]Coordination for the Improvement of Higher Education Personnel, Brasilia, DF, BRA, [6]North-West University Potchefstroom, Potchefstroom, NW, RSA, [7]Science Systems and Applications, Inc., Lanham, MD, USA, [8]Virginia Commonwealth University, Richmond, VA, USA, [9]City University of New York, New York, NY, USA, [10]LuftBlick Earth Observation Technologies, Kreith, Mutters, AUT

Abstract

Accurately capturing the evolution of episodic stratosphere-to-troposphere transport is critical due to the potential impacts on both climate and air quality. Until now, investigating associated spatiotemporal gradients in total column ozone (TCO) has primarily been the task of observations from polar-orbiting satellites as well as high-resolution models. We explore how a network of five ground-based Pandora spectrometer systems can be utilized in a similar fashion. The passage of a strong mid-latitude cyclone in March 2018 and its associated stratospheric intrusion is used as a case demonstrating the ability of networked Pandora observations to contextualize these regions of transport across space and time. Results show that the high temporal resolution of Pandora observations and the networked approach were able to resolve increases in TCO associated with stratosphere-to-troposphere transport and to capture the spatial context of the chosen episode. The use of networked Pandora observations shows promise for additional transport studies and for supporting future geostationary atmospheric composition satellite missions and modeling efforts.

1. Introduction

Downward transport of ozone (O_3) from the stratosphere to the troposphere is a long-established principal natural contributor to tropospheric O_3 (Singh et al., 1978). Accordingly, the frequency and strength of this transport have potential implications for both climate and air quality (Fiore et al., 2003). In fact, several studies have directly linked stratosphere-to-troposphere transport (STT) to observed surface O_3 exceedances (e.g., Kaldunski et al., 2017; Langford et al., 2009; Lin et al., 2012). Therefore, improving observations and modeling of STT continues to be an active area of research.

In the mid-latitudes particularly, STT is highly episodic and most often associated with synoptic scale wave features (Stohl et al., 2003). For example, surface cold fronts associated with mid-latitude cyclones are a key contributor to the prevalence of STT (Danielsen, 1968; Holton et al., 1995; Lamarque and Hess, 1994; Wirth and Egger, 1999) because they induce lowering of the tropopause beneath a jet circulating the area of low-pressure (Langford et al., 2017 and references therein). Further, STT mediated by mid-latitude cyclones has been shown to occur frequently during the winter to spring transition (Elbern et al., 1998), a period that coincides with maxima in lower stratospheric O_3 (Monks, 2000). These surface low-pressure systems are also accompanied by an upper-level trough that supports their development, steers their evolution, and aids in STT through the equatorward advection of O_3-rich air masses that are also poor in water vapor (Browning and Pardoe, 1973; Carlson, 1991; McClain, 1960). As they are advected, these air masses descend while wrapping cyclonically into the center of low-pressure and induce cloud-free conditions that are often referred to as the "dry slot" of the cyclone (Browning, 1997) (Figure 1b). STT is an additional consequence of their descent and, because they are O_3-rich as compared to their surroundings, their advection creates distinct spatial gradients in O_3. For these reasons, STT events have been shown to enhance satellite-derived total column O_3 (TCO) in their vicinity by 10-20 % between daily overpasses (e.g., Bonasoni et al., 2000; Stohl et al., 2000).

Most recently, researchers have benefitted from the higher resolution and improved representation of O_3 dynamics within models to explore STT (Knowland et al., 2017a,b; 2015; Ryoo et al., 2017; Škerlak et al., 2014) and have shown that mid-latitude cyclones can account for approximately half of all northern hemisphere (NH) STT of O_3 (Jaeglé et al., 2017). For decades before this, research relied on several additional approaches that leveraged sparsely located ground-based and in-situ techniques. Numerous investigations heavily utilized O_3 lidars, ozonesonde profiles, and surface O_3 monitors to investigate the influence of strong stratospheric intrusions (SIs) on air quality at higher elevations (e.g., Langford, 1999; Langford et al., 2012, 2009, 1996; Lefohn et al., 2011; Lin et al., 2012; Shapiro, 1980). For example, Lin et al. (2012) used all three of these observational datasets synergistically with models to estimate that a deep SI can contribute as much as 40 ppbv of O_3 to surface concentrations at sites in the intermountain west region of the United States (US). While studies centered on this array of observational datasets are less prevalent now in favor of modeling approaches, recent advances in ground-based, direct-sun remote sensing of O_3 may provide novel insight on STT episodes.

To identify spatial TCO gradients and thus potential regions of STT, observations from polar-orbiting satellite platforms retrieving TCO have been a primary tool (e.g., Knowland et al., 2017a; Olsen et al., 2000; Ott et al., 2016). The power of these observations is their near-global coverage and ability to often conduct retrievals even near the complex cloud structure of mid-latitude cyclones (Susskind et al., 2006). However, temporal resolution is a noted limitation due to overpasses only occurring once or twice daily. Fully exploring the evolution of STT episodes may therefore benefit from the use of ground-based observational datasets with enhanced temporal resolution. This was demonstrated by Fioletov (2008), who provided a case study demonstrating the ability to track rapid lowering of the tropopause and associated TCO enhancements on sub-daily timescales with observations from a ground-based radar and Brewer spectrophotometer.

March 2018 was a period of frequent cyclogenesis over the eastern US, typical as the winter transitions to spring. The passage of a mid-latitude cyclone during the period of 13-14 March 2018 and its likely associated STT is used to answer the scientific question: *can a small number of networked, ground-based Pandora spectrometer systems in the northeast US effectively resolve the highly dynamic TCO features associated with STT*? The combination of ground-based, space-based, and modeled datasets used in this analysis are described in detail in Section 2. In Section 3, we compare Pandora observations to the ancillary datasets to contextualize this episodic transport and to highlight differences in how each platform resolved the chosen case. Conclusions are presented in Section 4.

2. Datasets and Methods

2.1. Ground-Based Observational Datasets

2.1.1. Pandora

Pandora is a ground-based UV–Visible spectrometer system capable of columnar direct-sun and moon observations as well as sky-scanning profiles (Cede, 2017; Herman et al., 2009). Pandora direct-sun TCO data are reported to an accuracy of ± 15 Dobson units (DU, where 1 DU = 2.69×10^{16} molecules cm^{-2}; Müller et al., 2017). Spectra collected by Pandora instruments are analyzed using a Differential Optical Absorption Spectroscopy technique (DOAS; Platt and Stutz, 2008). Under standard direct-sun operations, Pandora provides a TCO data point approximately every 120 seconds. Additionally, the turnaround time for data processing (within approximately 10 minutes of spectra being measured in the field; Müller et al., 2017) provides the possibility of using observations to monitor the spatiotemporal evolution of TCO associated with STT in near real-time. Currently, only the direct-sun observation mode of Pandora has been extensively validated against other ground- and space-based remote sensing platforms (e.g., Baek et al., 2017; Herman et al., 2015; Reed et al., 2013; Tzortziou et al., 2012). Thus, this analysis is limited to hourly averaged (matching the temporal resolution of the model dataset) Pandora direct-sun TCO observations.

At each site, Pandora data were filtered for clouds and algorithmic error according to Tiefengraber and Cede (2017) by excluding data points with a normalized weighted root-mean squared spectral fitting residual $>8\times10^{-3}$ and a reported uncertainty >15 DU. This filtering was mostly driven by cloud conditions throughout the month and resulted in the removal of approximately 40 % of the total observations at each site. Despite this, temporal gaps in the Pandora dataset that would be detrimental to contextualizing STT do not exist for March 2018 due to STT being confined to the dry, cloud-free environment to the west of each cyclone.

Between 2016 and early 2019, the number of Pandora systems sited globally expanded beyond 75 as part of the emerging National Aeronautics and Space Administration (NASA) and European Space Agency (ESA) cooperative Pandonia Global Network (PGN; Swap et al., 2018). For this study, observations from five Pandora systems sited at locations throughout the northeast US were used. These sites and their coordinates are given in Figure 1a and from south to north are: Pandora #38 at NASA Langley Research Center (LaRC); Pandora #40 at the Virginia Commonwealth University Rice Rivers Center (VCU); Pandora #32 at NASA Goddard Space Flight Center (GSFC); Pandora #19 at University of Maryland, Baltimore County (UMBC); and Pandora #135 at the City College of New York (CCNY). Additionally, Figure 1 shows these sites with true color imagery (Figure 1a-b) and total column water vapor imagery (Figure 1b) on 13 March 2018 from the Moderate Resolution Imaging Spectrometer (MODIS) onboard NASA's Terra satellite. This imagery emphasizes not only the cloud structure of the cyclone but also the relatively dry and cloud-free conditions over the southeast US.

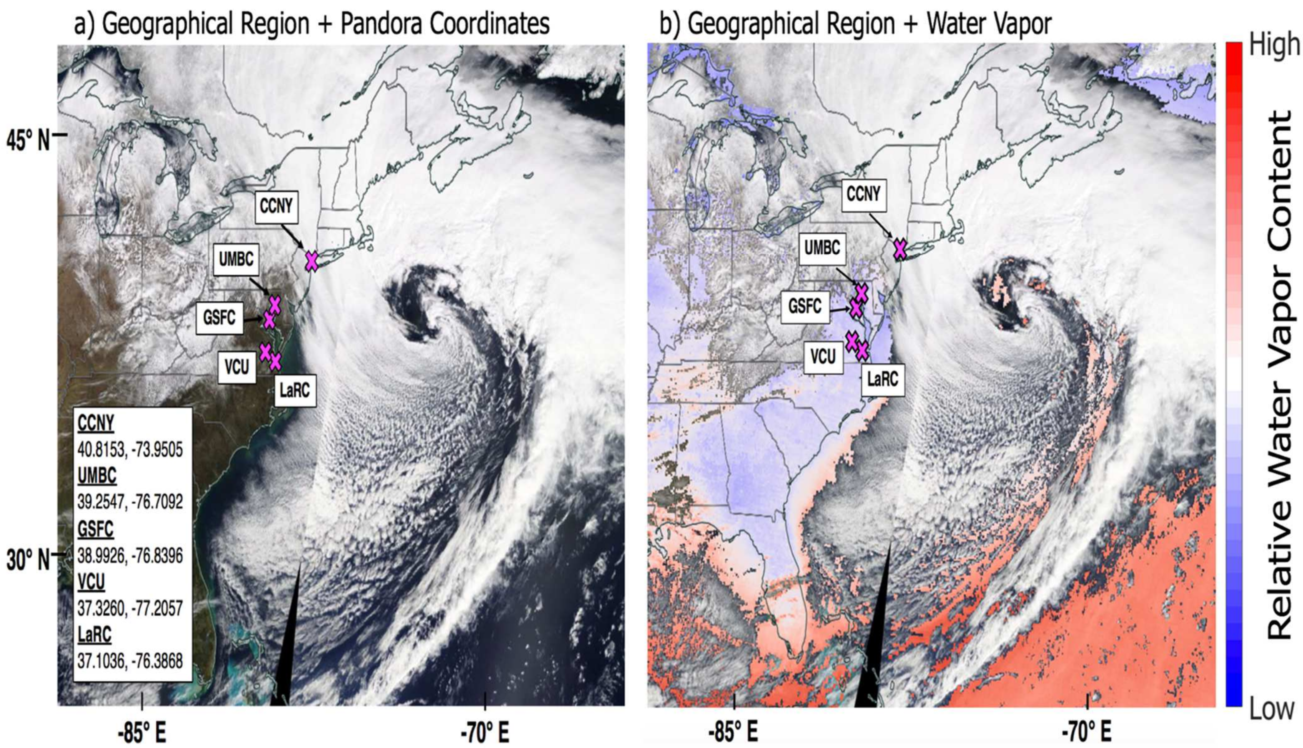

Figure 1 **(a)** True color imagery on 13 March 2018 from the Moderate Resolution Imaging Spectrometer (MODIS) onboard NASA's Terra satellite (accessed 06 December 2018 from https://worldview.earthdata.nasa.gov/) emphasizes the presence of a mid-latitude cyclone (comma-shaped cloud feature) off the coast of the eastern US. Additionally, note the general lack of cloud cover over the eastern US to the west of the system. Pandora system locations, labels, and geographic coordinates are indicated (magenta crosses and list). **(b)** Similar to **(a)** with the inclusion of total column water vapor content from MODIS onboard Terra (accessed 18 September 2019 from https://worldview.earthdata.nasa.gov/). Blue shading represents low amounts of water vapor whereas red shading represents higher amounts of water vapor in the atmospheric column. Note the relatively low water vapor content over the eastern US study region and that water vapor content increases moving eastward across the cyclone.

Operating Pandora in direct-sun (i.e. sun tracking) mode provides capabilities for the chosen case that would not have been afforded by zenith-only observations. Primarily, direct-sun observations have the advantage of simplifying assumptions in the DOAS retrieval surrounding air mass factors (Platt and Stutz, 2008). However, direct-sun viewing geometries also allow for estimating the geographic location of maximum O_3 absorption for each Pandora observation and horizontally translating the data point to these "effective coordinates". While studies considering Pandora viewing geometries when making comparisons to airborne and polar-orbiting satellite measurements exist (e.g., Müller et al., 2017; Nowlan et al., 2018; Spinei et al., 2018; see also Verhoelst et al., 2015), the use of effective coordinates has potentially enhanced utility for comparisons to more continuous datasets such as model outputs and geostationary satellite observations. It should also be noted that effective coordinates are most applicable during investigations of O_3, and more specifically TCO, due to the nature of O_3 maxima occurring in the stratosphere and not near-surface (e.g., as with species such as nitrogen dioxide and formaldehyde).

The effective coordinates of each hourly-averaged Pandora TCO data point are calculated using its corresponding hourly-averaged solar zenith and azimuth viewing angles (e.g., Müller et al., 2017) and an assumed maximum in O_3 absorption at an altitude of 22 km (compare to e.g., Bernhard et al., 2005) (Figure 2). Note this altitude will vary depending on latitude, however for NH hemisphere mid-latitudes this assumption is valid. Further, while STT events do bring O_3 from the lower stratosphere down into the troposphere, maxima in O_3 remain well into the stratosphere and this assumption remains valid even during such an event. For example, in the morning and afternoon, direct-sun Pandora data are measured at a moderate to high solar zenith angle (i.e. low solar elevation angle). Thus, for a system in the NH mid-latitudes the effective coordinates may be shifted approximately 100 km (or approximately 1°) to the southeast of the physical ground location in the morning, by a very small value around solar noon, and approximately 100 km (or approximately 1°) to the southwest in the evening. Figure 2 provides a schematic of how this geographic translation occurs as a function of Pandora viewing geometries in the afternoon.

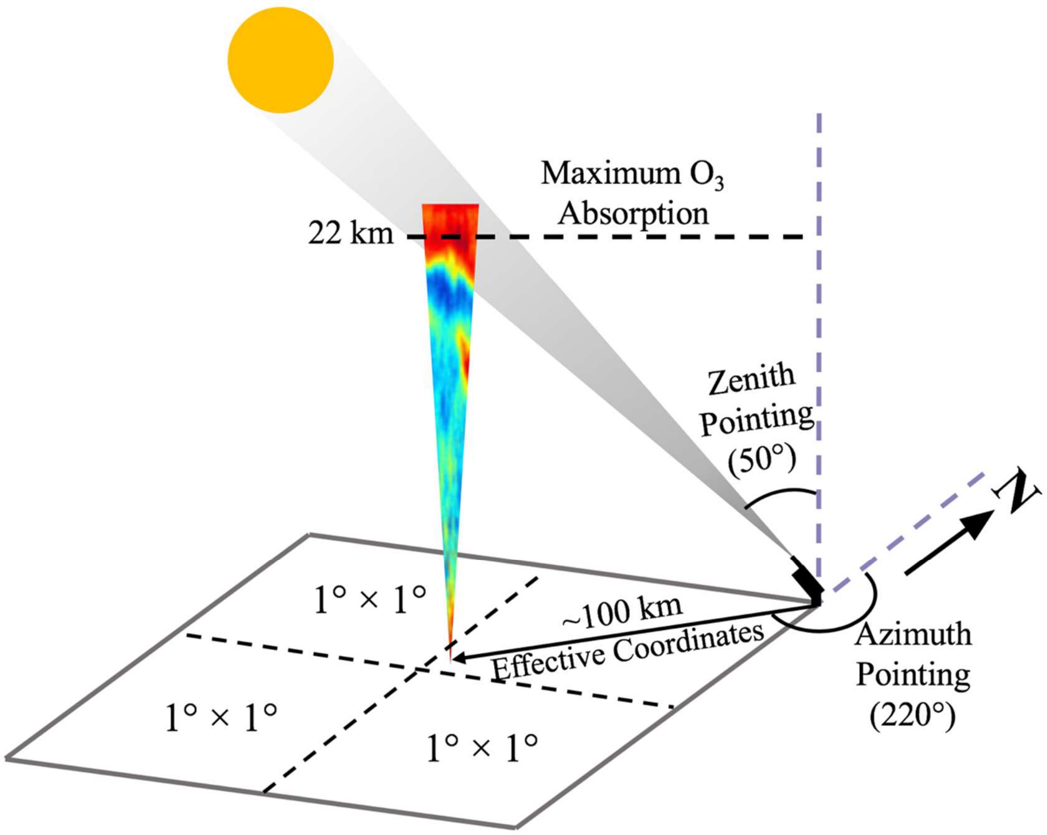

Figure 2 Schematic of Pandora direct-sun viewing geometry and relation to effective coordinates. Each quadrant of the projected surface region approximately represents a 1° × 1° sized grid box. An example ozone lidar curtain is given highlighting that the largest ozone concentrations (red shading) are present in the stratosphere (see https://www-air.larc.nasa.gov/missions/TOLNet/ for additional examples). Example Pandora zenith and azimuth viewing angles are given for a NH mid-latitude site during the afternoon. Note that numbers given are not exactly to scale.

2.1.2. Brewer Spectrophotometer

The ground-based Brewer spectrophotometer (Kerr et al., 1984) has a long history of providing ground-based TCO observations aimed at validating TCO measured from space (e.g., Balis et al., 2007; Labow et al., 2013; McPeters et al., 2008). Coupled with a global distribution of more than 200 instruments, this has resulted in a widely used and trusted platform. Further, a Brewer instrument provides high fidelity TCO observations on a timescale that most matches Pandora (i.e. sub-hourly) and is therefore extremely valuable for evaluating Pandora. Hourly TCO from a Brewer sited at GSFC and the GSFC Pandora compared very favorably throughout the entire month of March 2018 ($R^2 = 0.98$) and even during the dynamic TCO conditions of the chosen case study (e.g., the Pandora and Brewer were within 3.3 % of each other across 13-14 March).

2.2. Space-based Observational Datasets

2.2.1. Ozone Mapping Profiler and Suite (OMPS)

The Ozone Mapping and Profiler Suite (OMPS), housed on the joint NASA/National Oceanic and Atmospheric Administration (NOAA) Suomi National Polar-Orbiting Partnership (NPP) satellite, is composed of three instruments: the nadir mapper, nadir profiler, and limb profiler (Flynn et al., 2014). For the L3 V2 product mentioned above, the nadir mapper, or OMPS-NM, measures TCO globally with a horizontal resolution of 1^o. Flynn et al. (2014) additionally showed the performance of OMPS to be consistent, with TCO values within approximately 3 % compared to other satellite and ground-based TCO observations. Here, OMPS TCO is used as an initial tool to evaluate the bias of each Pandora system in an effort to establish relative Pandora performance for March 2018.

Comparisons of level 3 version 2 (L3 V2) daily TCO from OMPS and Pandora observations coincident with OMPS afternoon overpasses (approximately 17-18 UTC or 13 local time) during March 2018 found no significant difference in individual Pandora biases (biases relative to OMPS ranging from -2.47 % to -0.43 %, average -1.24 %). This consistency across Pandora systems relative to both OMPS and Brewer adds additional confidence in the performance of the instruments and resulting data for their use in contextualizing the chosen STT episode.

2.2.2. Atmospheric Infrared Sounder (AIRS)

For this investigation, daily TCO from the Atmospheric Infrared Sounder (AIRS; Aumann et al., 2003) onboard NASA's Aqua satellite is used. Although TCO is retrieved in order to improve the quality of other AIRS products (e.g., temperature), it has been shown to be a useful standalone product (e.g., Monahan et al., 2007). Here, the AIRS level 3 version 6 (L3 V6) TCO retrieval is used and has a 1° horizontal resolution (Susskind et al., 2014). AIRS often has usable data even in the presence of clouds due to its rigorous cloud-clearing procedure. In brief, the cloud-clearing procedure determines information about the amount of cloud cover and altitude of multiple cloud layers (see Susskind et al., 2014; 2006 for additional detail). In cloudy scenes, this procedure ultimately allows AIRS to generate radiances that would be measured under clearer conditions.

For the period of the presented case study there were satellite TCO observations available from OMPS, AIRS, and also the Ozone Monitoring Instrument (OMI) aboard NASA's Aura satellite. To examine day-to-day variability in March 2018 TCO and to evaluate the enhanced temporal resolution of Pandora observations, AIRS is chosen over the other mentioned platforms for the following reasons. Firstly, AIRS is not assimilated into the utilized model dataset while OMI is, thus eliminating OMI as an independent observational dataset. It should also be noted that OMPS TCO is ingested into the Goddard Earth Observing System (GEOS) forecast systems (see https://gmao.gsfc.nasa.gov/GMAO_products/NRT_products.php#) and is likely moving towards being ingested into global reanalyses. Secondly, recent investigations of SIs in the US have also used AIRS as a satellite dataset independent to any modeling efforts (e.g., Knowland et al., 2017a; Ott et al., 2016) due to its twice-daily overpass and ability to conduct retrievals in cloudy scenes. Finally, although OMPS compared well to Pandora for March 2018, the ultimate goal of this investigation is to highlight differences in resolving STT events between observational and model platforms and not to shift the focus to strictly validating each platform. For this investigation, the AIRS TCO value from the grid cell nearest the Pandora physical ground location is taken because at the time of the daytime AIRS overpass, and when averaged over the entire day, the effective Pandora coordinates are only a small distance (and within the same AIRS pixel) from the physical ground location.

2.3. Model Datasets

2.3.1. The NASA Modern Era Retrospective analysis for Research and Applications, version 2 (MERRA-2) Reanalysis

The NASA Modern Era Retrospective analysis for Research and Applications, version 2 (MERRA-2; Gelaro et al., 2017) reanalysis is a robust dataset for examining overall synoptic conditions during the development and passage of the 13-14 March mid-latitude cyclone case as well as its mediation of STT. MERRA-2 is output on a high-resolution global grid ($0.5^{o} \times 0.625^{o}$ latitude-by-longitude), on 72 model layers up to 0.01 hPa, and spans the timeframe from 1980 to within a few weeks of the present. Additionally, MERRA-2 assimilates meteorological, aerosol, and O_3 observations using the Goddard Earth Observing System data assimilation system (Bosilovich et al., 2015; Gelaro et al., 2017; McCarty et al., 2016). Notably, beginning in late 2004 MERRA-2 assimilates retrievals of TCO from OMI (Levelt et al., 2006) and O_3 profiles in the stratosphere from the Microwave Limb Sounder (Waters et al., 2006), also aboard NASA's Aura satellite (Bosilovich et al., 2015; Gelaro et al., 2017; McCarty et al., 2016). Recent work by Knowland et al. (2017) showed that despite simplification of chemistry in the troposphere (Ott et al., 2016), MERRA-2 is a useful tool for investigating the fine-scale structure of SIs and their potential impacts on surface O_3 and air quality. We believe the potential for contextualizing STT episodes provided by the combination of datasets and approaches used in this investigation complements those recent findings and may help to guide future developments in the synergistic use of compositional observations and reanalyses.

Here, daily averages of the following MERRA-2 meteorological fields are used on pressure levels up to 150 hPa – winds (u, v), sea-level pressure, geopotential height, relative humidity (RH), equivalent potential temperature (θ_e; calculated using temperature and specific humidity), and Ertel's potential vorticity (Global Modeling and Assimilation Office (GMAO), 2015a, 2015b). In addition, a daily-averaged estimate of the dynamical tropopause is calculated based on the two potential vorticity unit (PVU) isosurface (Holton et al., 1995), where 1 PVU = 10^{-6} K m^2 kg^{-1} s^{-1}. Hourly-averaged assimilated TCO from MERRA-2 (GMAO, 2015c) is extracted for comparisons against Pandora observations and as an ancillary tool for contextualizing the overall STT episode. For comparisons, the hourly MERRA-2 TCO value from the grid cell nearest the Pandora effective location for the same hour is used. This is in contrast to AIRS TCO because

Pandora effective coordinates change relative to the ground location more on an hourly basis than when averaged over the entire day.

3. Results and Discussion

3.1 Synoptic Conditions With MERRA-2

On 13-14 March 2018, an intense mid-latitude cyclone moved northeastward along the US east coast, as depicted by the MERRA-2 daily-averaged synoptic meteorology (Figure 3). On 13 March, there was a strong low-pressure area off the coast of the eastern US with an extensive cold-front (Figure 3a). Behind the surface cold-front, the descent of stratospheric air is expected to be accompanied by relatively dry conditions (Browning and Roberts, 1994; Knowland et al., 2015; Young et al., 1987). This feature was captured in MERRA-2 700 hPa RH (Figure 3a) by an area of RH <30 % covering much of the central and southeast US. Note that another, weaker surface low-pressure area was also present over New York and Lake Ontario (Figure 3a).

An upper-level trough was revealed in MERRA-2 geopotential heights at 500 hPa on 13 March (Figure 3b) as a widespread area of <530 decameters (dam) over the Great Lakes region. MERRA-2 additionally captured regions of opposing northerly ($v < -15\ ms^{-1}$) and southerly ($v > 25\ ms^{-1}$) winds that reached the lower troposphere (Figure 3c). This feature steered TCO gradients by aiding the advection of O_3-rich polar air towards the northeast US (Figure 3c). This air mass was seen in the daily-averaged MERRA-2 TCO as an area >395 DU over the central US (Figure 3b). On 13 March the SI associated with this storm had not yet become organized into deep and widespread feature over the northeast (e.g., Appenzeller and Davies, 1992; Knowland et al., 2017b, 2015) due to it primarily being associated with the western edge of the weaker low-pressure area and trough. However, a lowering of the tropopause from approximately 200 hPa on 12 March (not shown) to an altitude of about 350 hPa on 13 March was captured in MERRA-2 over all of the Pandora systems (Figure 3c).

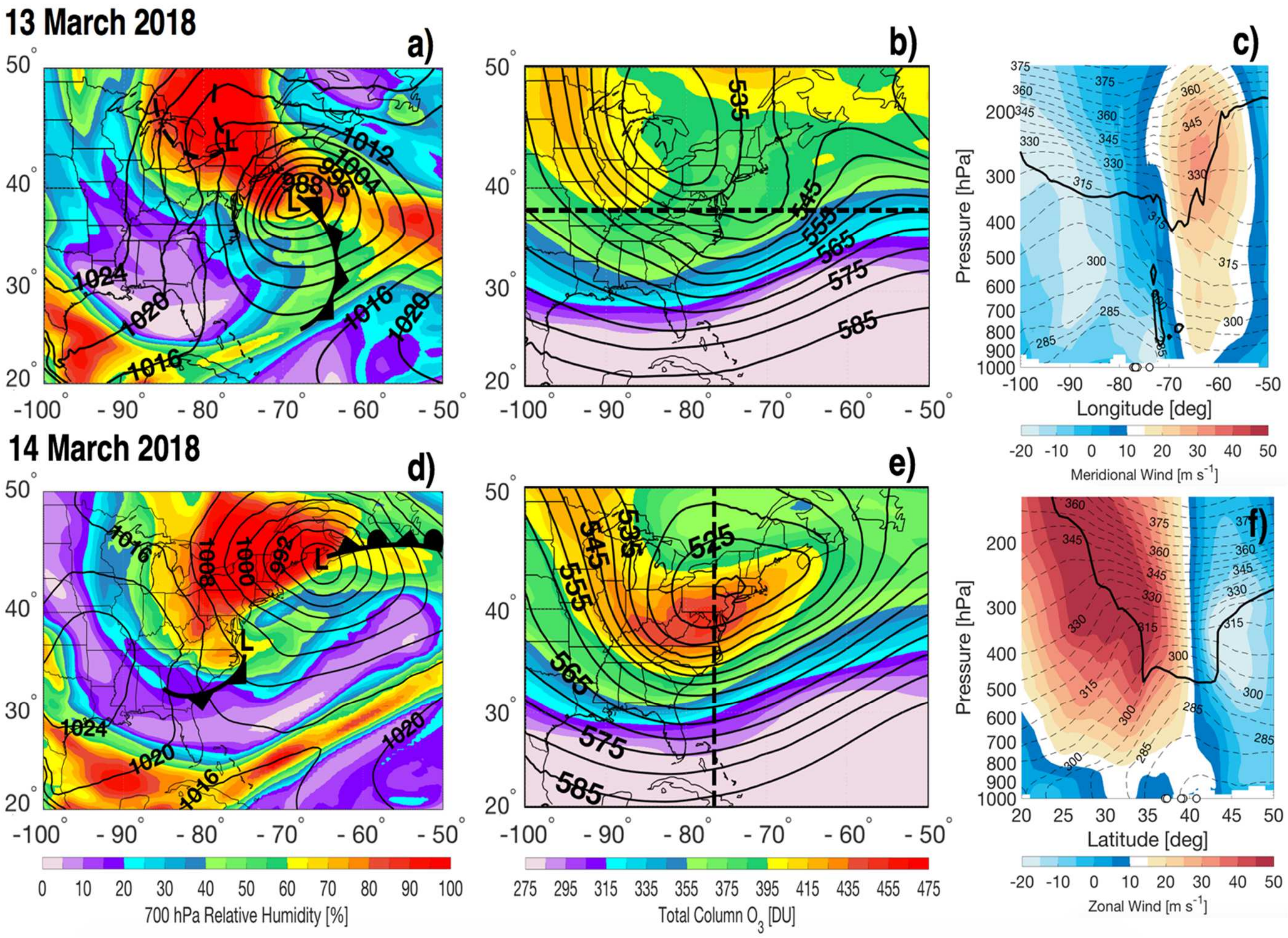

Figure 3 Daily-averaged synoptic conditions over the eastern US from 13 March (a-c) and 14 March (d-f) 2018 using the MERRA-2 reanalysis. **(a and d)** 700 hPa relative humidity (shading; %), sea level pressure (black contours; 4 hPa intervals), and approximate location of low-pressure centers and frontal boundaries from daily National Weather Service surface analyses (taken from https://www.wpc.ncep.noaa.gov/dailywxmap/, *Accessed* 19 March 2019). Note, not all frontal features have been depicted. Cold fronts (black line with triangles), surface troughs (black dashed lines), and occluded fronts (black line with alternating triangles and half-circles) are shown. **(b and e)** Daily-averaged MERRA-2 TCO (shading; DU) and 500 hPa geopotential height (contours; 5 dam intervals). Black dashed lines represent the vertical transects provided in panels c and f. **(c and f)** Daily-averaged vertical transects along 38º N from 100º W to 50º W for 13 March 2018 **(c)** and along 76º W from 20º N to 50º N for 14 March 2018 **(f)** over the northeast US (Pandora ground locations given by white circles). Meridional (**c** shading; ms^{-1}) and zonal (**f** shading; ms^{-1}) winds are shown along with θ_e (dashed contour lines, 5 K intervals) and the 2 PVU isosurface (thick black contour).

Based on surface analyses for 14 March, the stronger area of low-pressure had moved to the coast of Maine, merging with the weaker low-pressure area over New York from the previous day (Figure 3d). Further, because of the marked frontal occlusion, the dry slot had wrapped deeper into the cyclone center (Figure 3d). While conditions over the southeast US were not as dry as the day previous (RH >50 %; Figure 3d), surface analyses showed another, weaker surface low had developed off the coast of Virginia with its own associated cold front (Figure 3d). Additionally, a new minimum in 500 hPa geopotential height of 520 dam occurred over New York (Figure 3e). MERRA-2 winds highlighted a jet over the study area as strong westerly (u

>45 ms^{-1}) flow that connected down to the lower troposphere (Figure 3f). In addition, there was relatively tight packing of isotherms between 30º N and 35º N (Figure 3f) indicative of the offshore cold-front. The area of elevated TCO (>450 DU) also now covered the entire northeast region (Figure 3d) as did the lowering of the tropopause (down to about 500 hPa; Figure 3f). Coupled with the frontal occlusion, this allowed the O_3-rich air mass to wrap cyclonically into the center of low-pressure, enhancing spatial TCO gradients across the region (Browning, 1997; Carlson, 1991) (Figure 3e).

3.2 Temporal Evolution of TCO

As mentioned previously, March 2018 was a particularly active period for mid-latitude disturbances in the North Atlantic sector. Rapid increases in TCO are expected to coincide with the passage of each storm as a result of advection of O_3-rich polar air masses towards the mid-latitudes (Browning and Pardoe, 1973; Carlson, 1991; McClain, 1960). Figure 4 shows TCO timeseries from Pandora, Brewer (GSFC only), AIRS, and MERRA-2 for all of March 2018 at GSFC and for the 13-14 March case specifically at all other stations. The timeseries for GSFC illustrates the dynamic TCO conditions in March 2018 associated with the frequent cyclone activity. Examining all stations together provides the opportunity to evaluate how the temporal evolution of TCO is captured during each STT episode by the high resolution of Pandora and MERRA-2 (both hourly) compared to AIRS (daily).

Despite the very dynamic TCO conditions, MERRA-2 TCO and Pandora observed TCO compared favorably at all sites (R^2 values on the order of 0.9 across sites; Figure 4). During these times, there were sharp increases preceding each STT episode across all locations and datasets. For the episode of interest, Pandora systems observed an average increase of 26 DU in only 8 hours on 13 March (Figure 4). Across all five Pandoras, this corresponded to an average increase of 6 %, broadly consistent with previous findings from space-based TCO observations (e.g., Bonasoni et al., 2000; Stohl et al., 2000). Though AIRS captured the overall variability in TCO throughout the month, including the STT episodes, the timing of each episode was lost due to its daily temporal resolution. Pandora is able to capture TCO variability outside of satellite overpass times at a high temporal resolution and is therefore better suited to track the fine-scale temporal evolution of each particular episode.

Overall elevated TCO (>450 DU) on 14 March was captured by all datasets at all sites (Figure 4). These conditions were indicative of the advected O_3-rich air and STT mediated by the previously mentioned merged areas of low-pressure (Figure 3). Comparing Pandora as well as MERRA-2 to AIRS on 14 March, there appears to be a positive bias of approximately 10 % in the AIRS TCO value at every site except CCNY (Figure 4). This positive bias was observed throughout March 2018 but became most prevalent during the four STT events (Figure 4a). In comparisons to ozonesondes, Monahan et al. (2007) showed that AIRS tends to overestimate upper tropospheric O_3. This bias may be exacerbated by STT and its creation of complex O_3 conditions in the upper troposphere and lower stratosphere. Nevertheless, Monahan et al. show that AIRS TCO agrees to within a few percent of Total Ozone Mapping Spectrometer (TOMS) TCO. We find similar results for March 2018 when comparing AIRS and Pandora across all sites (AIRS biases relative to Pandora ranging from +2.43 % to +7.52 %, average +4.41 %). The high bias in AIRS TCO during the chosen STT event is an additional example highlighting the need for more than a daily snapshot from space-based platforms when exploring the spatiotemporal evolution of STT.

On 14 March MERRA-2 TCO underestimated the observed Pandora values by an average of 1.39 % across all sites (Figure 4). This underestimation was observed throughout the month and is consistent with previous findings from Wargan et al. (2017). The ability to resolve rapid increases in TCO as well as persistence of elevated TCO corresponding to STT demonstrates the promise of Pandora as a high temporal resolution tool to be used in addition to space-based platforms for exploring STT episodes.

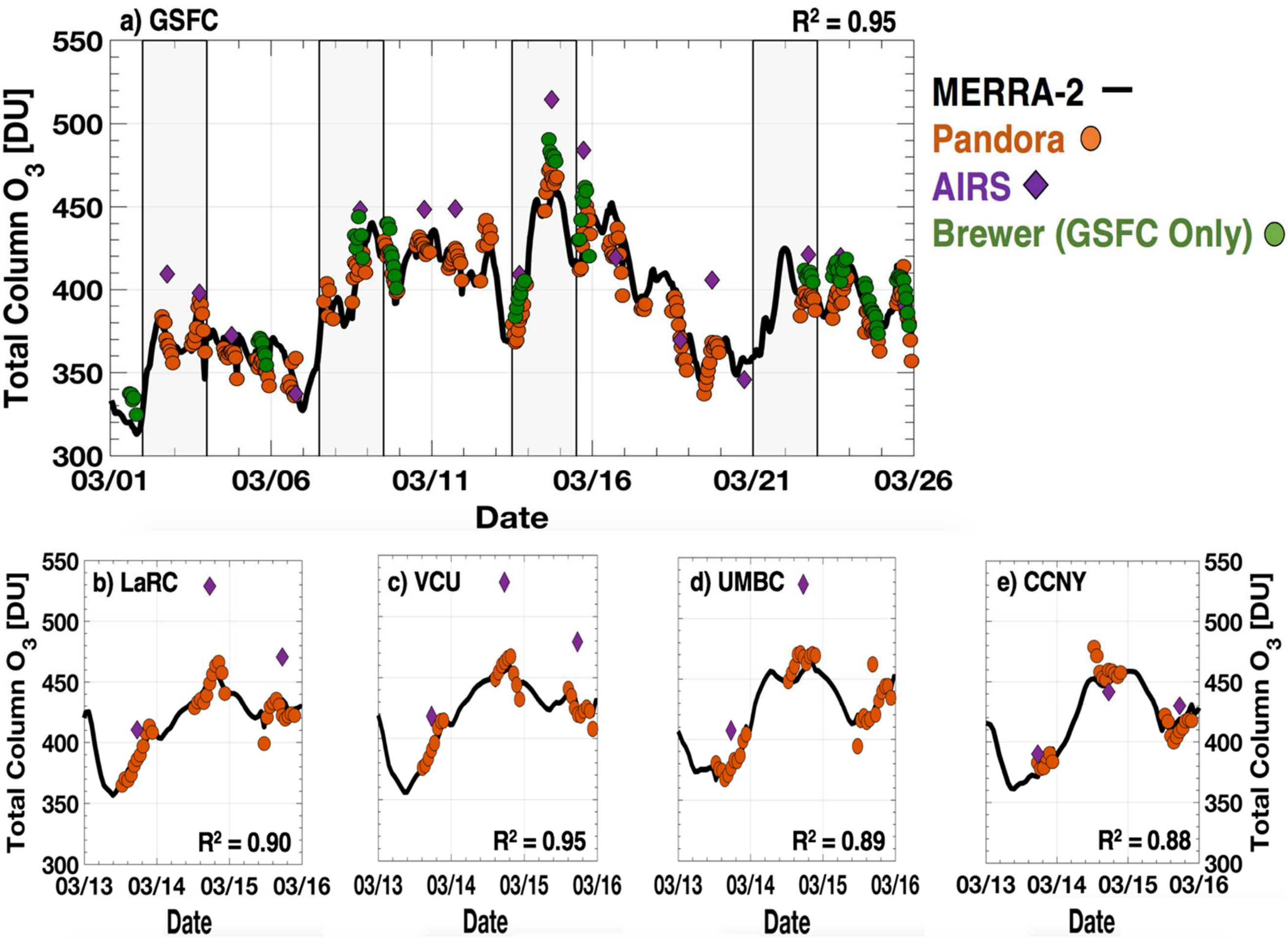

Figure 4 TCO time series from Pandora (hourly; orange points), AIRS (daily taken from grid cell closest to Pandora ground location; purple diamonds), and MERRA-2 (hourly taken from grid cell closest to hourly Pandora effective coordinates; solid black line) at GSFC for 01-25 March 2018 and at all other sites for 13-15 March 2018. R^2 values for MERRA-2 to Pandora comparisons at each site are given as well. Gray inserts in panel a represent the approximate timing of passage of the four mid-latitude cyclones based on surface analyses and their associated increase in TCO. Hourly TCO data from a Brewer Spectrophotometer sited at GSFC are shown in panel c (green points). Timestamps for all plotted data are in UTC.

3.3 Spatial Evolution of TCO with Pandora and MERRA-2

MERRA-2 and AIRS were examined on 13 March at each site in order to assess the best candidate for spatially contextualizing the chosen STT event (Figure 4). For site pairs close in distance - whose effective coordinates at times may be in the same model or satellite grid box - 1) GSFC and UMBC and 2) VCU and LaRC, AIRS captured relatively small gradients of 3 DU and 9 DU, respectively (Figure 4a-d). The largest difference AIRS observed between sites on this day was 20 DU between LaRC (410 DU) and CCNY (390 DU) (Figure 1; 4b-e). This pronounced gradient is potentially useful for identifying the advected O_3-rich air mass on a larger scale. At the same time, MERRA-2 slightly underestimated these gradients compared to AIRS: 0 DU between GSFC and UMBC; 1 DU between VCU and LaRC; and 17 DU between LaRC and CCNY (Figure 4). Therefore, it seems that both datasets would yield similar results for contextualizing spatial features of STT. However, using MERRA-2 alongside Pandora affords the opportunity of assessing TCO gradients outside of the satellite overpass time and on an hour-by-hour basis.

Figure 5 shows representative hourly TCO distributions for 13 and 14 March from both the network of Pandora systems (plotted at their effective coordinates) and from MERRA-2 over the northeast study region. Networked Pandora observations provided the capability to not only quantify the sharp increases in TCO associated with STT but also capture the spatial extent of the 13-14 March episode over its duration. Examining TCO across both days provides the best case for highlighting the utility of these networked observations because it provided two distinct TCO setups as shown by the synoptic conditions (Figure 3). On 13 March MERRA-2 captured the leading edge of the O_3-rich air mass being advected over Virginia (Figure 5a-c). Consistent with MERRA-2, Pandora observations at CCNY, located at the far northern end of the study region, revealed the spatial extent of the air mass and its protruding eastern edge (Figure 5a-c). This was particularly evident at 19 UTC when the relatively fine leading edge of O_3-rich air was pronounced in MERRA-2 TCO and captured by Pandora TCO as 378 DU at CCNY compared to 409 DU at VCU (Figure 5a). Pandora TCO at GSFC (385 DU) and UMBC (382 DU) further revealed that the O_3-rich air was confined to the southern end of the study region (Figure 5a). Pandora observations in Virginia (LaRC and VCU) at 19 UTC on 13 March also captured spatial TCO gradients over a relatively short distance associated with the advected air mass (Figure 5a). At this time, the gradient between these two systems was 12 DU over a distance of approximately 70 km (Figure 5a). Although this gradient diminished to 6 DU at 20 UTC (Figure 5b) and then to 0 DU at 21 UTC (Figure 5c) due to the Pandora at LaRC capturing more of the O_3-rich air, the ability to resolve spatial differences in TCO over relatively small distances demonstrates the power of networked observations for exploring the spatial extent of STT episodes. Until now, this has been left solely to high-resolution satellites and models (Büker, 2005; Knowland et al., 2017a; Ott et al., 2016). Further, while the distance between the Pandoras at LaRC and VCU places them in adjacent MERRA-2 grid cells, these results pose the question for future work of whether or not a dense network of Pandoras can be used to investigate sub-pixel variability in both model and satellite datasets.

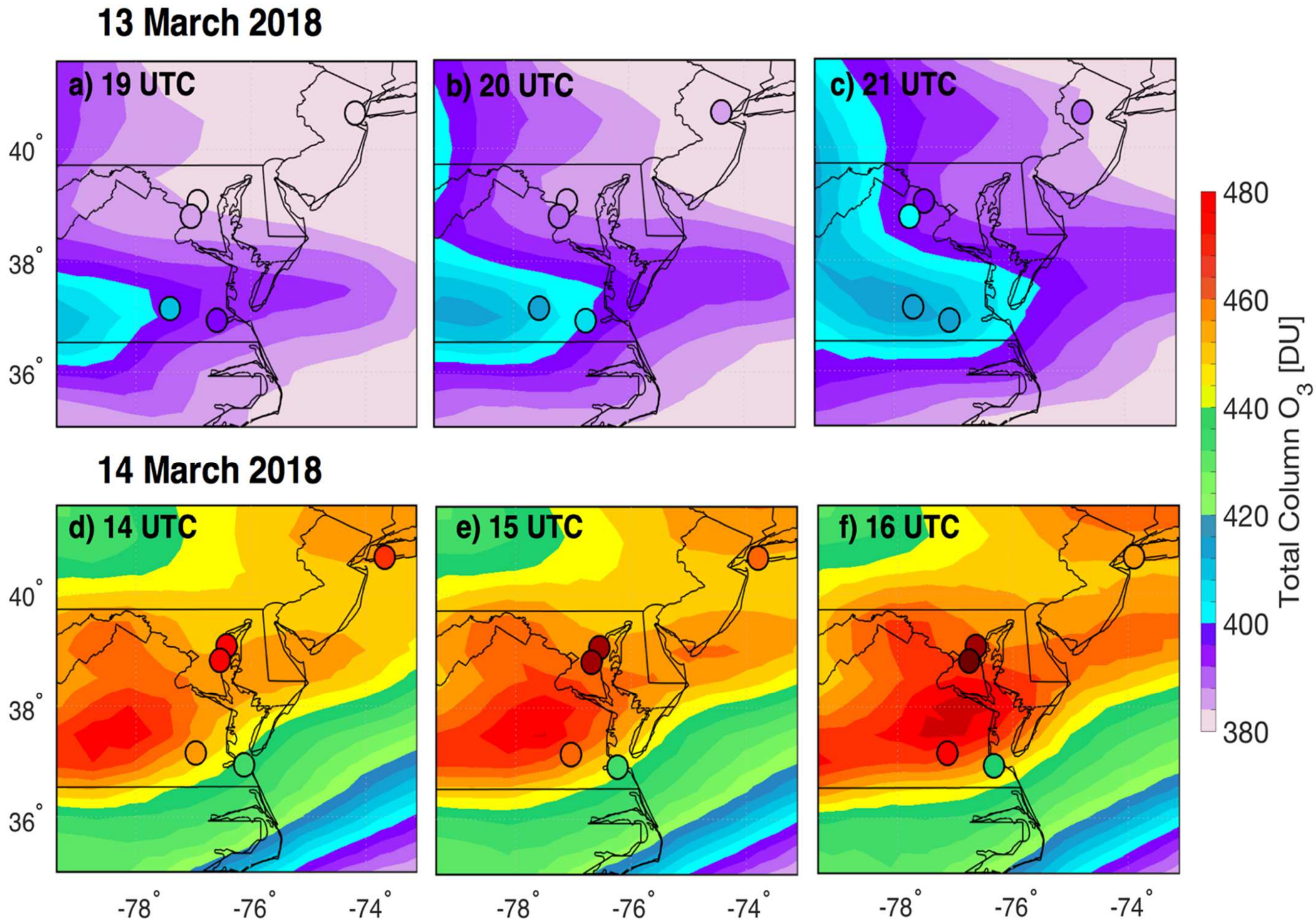

Figure 5 TCO observations from Pandora (colored points; plotted at effective coordinates) and assimilated TCO from MERRA-2 (shading) for 13 and 14 March 2018. **(a-c)** Hourly-averaged TCO from 19-21 UTC on 13 March 2018. **(d-f)** Hourly-averaged TCO from 14-16 UTC on 14 March 2018.

Contrasting TCO data from 19-21 UTC on 13 March and 14-16 UTC on 14 March highlight the setup of O_3-rich air over the northeast (Figure 5a-c) and its later wrapping into the low-pressure center (Figure 5d-f). During the 3-hour period shown from 14 March, there was persistence of elevated TCO (Figure 5d-f) captured by both Pandora and MERRA-2 across the entire region; and yet distinct gradients in TCO still existed between the southernmost Pandora systems at VCU and LaRC. Over the approximately 70 km distance between these sites, the Pandora systems captured gradients of 13 DU at 14 UTC; 22 DU at 15 UTC; and 21 DU at 16 UTC (Figure 5d-f). At the same times, MERRA-2 underestimated the gradient between these grid cells by factors of 2.6 (5 DU), 3.7 (6 DU), and 3.5 (6 DU) (Figure 5d-f). This underestimation was perhaps due to the fact that 14-16 UTC is before satellite overpass (i.e. before 13 local time) and thus before MERRA-2 can assimilate O_3 observations for the day. While there is no set threshold for how large spatial gradients in TCO must be in order to be associated with STT, frequent TCO observations from strategically sited Pandora systems appear to be a robust method for resolving these features.

4. Conclusions

The presented case study from March 2018 illustrates that a network of strategically deployed ground-based Pandora systems is able to capture both the spatial and temporal fine-scale structure of TCO variability associated with STT. While not providing the same global coverage as polar-orbiting satellites such as AIRS and a global reanalysis such as MERRA-2, the presence of multiple Pandora systems in a given region does serve to enhance the spatial context of STT and can be leveraged for identifying associated gradients in TCO. This was evident on 13 March when Pandora TCO helped reveal the leading edge of an O_3-rich air mass and again on 14 March when two Pandora systems captured a 22 DU gradient over a distance of approximately 70 km that MERRA-2 failed to similarly resolve. In addition, over the entire month of March 2018, agreement between MERRA-2 and Pandora systems across the northeast US was favorable despite highly dynamic conditions. This work highlights a new, expanded use case for Pandora and is encouraging a networked approach be used to conduct similar transport studies globally. Future work could explore the benefits gained from incorporating networked Pandora data into regional or global modeling efforts.

As atmospheric composition satellites continually improve in their spatial resolution (e.g., the Tropospheric Monitoring Instrument, TROPOMI; Veefkind et al., 2012), they become better equipped to identify the fine spatial structure of synoptic transport. Further, the upcoming geostationary mission Tropospheric Emissions: Monitoring Pollution (TEMPO; Zoogman et al., 2017) will usher in a new era of space-based remote sensing by providing high-resolution atmospheric composition observations on an hourly basis. Expansion of the PGN in support of validation and research activities surrounding both TROPOMI and TEMPO can be tailored to also opportunistically capture additional cases of STT. This could be accomplished by siting systems in areas of known cyclogenesis (e.g., the plains and northeast regions of the US; Harnik and Chang, 2003 and references therein) and optimizing their spacing for satellite comparisons. This would also serve the purpose of maximizing opportunities for capturing TCO gradients across both space and time.

Acknowledgements

This work was conducted under the NASA Pandora Project with funding support from the NASA Tropospheric Chemistry Program. Siting of the Pandora system at CCNY was supported by NASA grant number 80NSSC18K1035 with additional support from NOAA Earth System Sciences and Remote Sensing Technologies award number NA16SEC4810008. Analysis of networked Pandora data is only possible thanks to the involvement and support of global PGN members, Lena Shalaby (JCET/GSFC) and Alexander Dimov (SSAI/GSFC) from the NASA Pandora Project, as well as M. Müller (LuftBlick) from ESA Pandonia. Additionally, J. Robinson would like to thank Krzysztof Wargan (SSAI/GSFC) for useful discussions surrounding MERRA-2 data handling and analysis.

Data Availability

As central PGN data archiving and distribution services become available, Pandora data used in this investigation are available through the ESA Pandonia online archive (lb3.pandonia.net). MERRA-2, AIRS, and OMPS data are available through the NASA GES DISC online archive (https://disc.gsfc.nasa.gov/).

References

Appenzeller, C., Davies, H.C., 1992. Structure of stratospheric intrusions into the troposphere. Nature 358, 570–572. https://doi.org/10.1038/358570a0

Aumann, H.H., Chahine, M.T., Gautier, C., Goldberg, M.D., Kalnay, E., McMillin, L.M., Revercomb, H., Rosenkranz, P.W., Smith, W.L., Staelin, D.H., Strow, L.L., Susskind, J., 2003. AIRS/AMSU/HSB on the aqua mission: design, science objectives, data products, and processing systems. IEEE Trans. Geosci. Remote Sens. 41, 253–264. https://doi.org/10.1109/TGRS.2002.808356

Baek, K., Kim, J.H., Herman, J.R., Haffner, D.P., Kim, J., 2017. Validation of Brewer and Pandora measurements using OMI total ozone. Atmos. Environ. 160, 165–175. https://doi.org/10.1016/j.atmosenv.2017.03.034

Balis, D., Kroon, M., Koukouli, M.E., Brinksma, E.J., Labow, G., Veefkind, J.P., McPeters, R.D., 2007. Validation of Ozone Monitoring Instrument total ozone column measurements using Brewer and Dobson spectrophotometer ground-based observations. J. Geophys. Res. Atmos. 112, 1–10. https://doi.org/10.1029/2007JD008796

Bernhard, G., Evans, R.D., Labow, G.J., Oltmans, S.J., 2005. Bias in Dobson total ozone measurements at high latitudes due to approximations in calculations of ozone absorption coefficients and air mass. J. Geophys. Res. 110, D10305. https://doi.org/10.1029/2004JD005559

Bonasoni, P., Evangelisti, F., Bonafe, U., Ravegnani, F., Calzolari, F., Stohl, A., Tositti, L., Tubertini, O., Colombo, T., 2000. Stratospheric ozone intrusion episodes recorded at Mt. Cimone during the VOTALP project: case studies. Atmos. Environ. 34, 1355–1365. https://doi.org/10.1016/S1352-2310(99)00280-0

Bosilovich, M.G., Akella, S., Coy, L., Cullather, R., Draper, C., Gelaro, R., Kovach, R., Liu, Q., Molod, A., Norris, P., Wargan, K., Chao, W., Reichle, R., Takacs, L., Vikhliaev, Y., Bloom, S., Collow, A., Firth S., Labow, G., Partyka, G., Pawson, S., Re, M., 2015. MERRA-2: Initial evaluation of the climate. NASA/TM–2015–104606 43, 139.

Browning, K.A., 1997. The dry intrusion perspective of extra-tropical cyclone development. Meteorol. Appl. 4, S1350482797000613. https://doi.org/10.1017/S1350482797000613

Browning, K.A., Pardoe, C.W., 1973. Structure of low-level jet streams ahead of mid-latitude cold fronts. Q. J. R. Meteorol. Soc. 99, 619–638. https://doi.org/10.1002/qj.49709942204

Browning, K.A., Roberts, N.M., 1994. Structure of a frontal cyclone. Q. J. R. Meteorol. Soc. 120, 1535–1557. https://doi.org/10.1002/qj.49712052006

Büker, M.L., 2005. Resolution dependence of cross-tropopause ozone transport over east Asia. J. Geophys. Res. 110, D03107. https://doi.org/10.1029/2004JD004739

Carlson, T.N., 1991. Mid-Latitude Weather Systems. New York, NY, USA: Routledge, Chapman Hall, Inc.

Cede, A., Dec. 2017. Manual for Blick Software Suite 1.5. Luftblick Earth Observation Technologies. http://pandonia.net/media/documents/BlickSoftwareSuite_Manual_v9.pdf

Danielsen, E.F., 1968. Stratospheric-Tropospheric Exchange Based on Radioactivity, Ozone and Potential Vorticity. J. Atmos. Sci. 25, 502–518. https://doi.org/10.1175/1520-0469(1968)025<0502:STEBOR>2.0.CO;2

Elbern, H., Hendricks, J., Ebel, A., 1998. A Climatology of Tropopause Folds by Global Analyses. Theor. Appl. Climatol. 59, 181–200. https://doi.org/10.1007/s007040050023

Fioletov, V.E., 2008. Ozone climatology, trends, and substances that control ozone. Atmos. - Ocean 46, 39–67. https://doi.org/10.3137/ao.460103

Fiore, A., Jacob, D.J., Liu, H., Yantosca, R.M., Fairlie, T.D., Li, Q., 2003. Variability in surface ozone background over the United States: Implications for air quality policy. J. Geophys. Res. Atmos. 108, 4787. https://doi.org/10.1029/2003JD003855

Flynn, L., Long, C., Wu, X., Evans, R., Beck, C.T., Petropavlovskikh, I., McConville, G., Yu, W., Zhang, Z., Niu, J., Beach, E., Hao, Y., Pan, C., Sen, B., Novicki, M., Zhou, S., Seftor, C., 2014. Performance of the Ozone Mapping and Profiler Suite (OMPS) products. J. Geophys. Res. Atmos. 119, 6181–6195. https://doi.org/10.1002/2013JD020467

Gelaro, R., McCarty, W., Suárez, M.J., Todling, R., Molod, A., Takacs, L., Randles, C.A., Darmenov, A., Bosilovich, M.G., Reichle, R., Wargan, K., Coy, L., Cullather, R., Draper, C., Akella, S., Buchard, V., Conaty, A., da Silva, A.M., Gu, W., Kim, G.-K., Koster, R., Lucchesi, R., Merkova, D., Nielsen, J.E., Partyka, G., Pawson, S., Putman, W., Rienecker, M., Schubert, S.D., Sienkiewicz, M., Zhao, B., 2017. The Modern-Era Retrospective Analysis for Research and Applications, Version 2 (MERRA-2). J. Clim. 30, 5419–5454. https://doi.org/10.1175/JCLI-D-16-0758.1

[dataset] Global Modeling and Assimilation Office (GMAO) (2015a). MERRA-2 Inst3_3d_asm_Np: 3d,3-Hourly, Instantaneous, Pressure-Level, Assimilation, Assimilated Meteorological Fields V5.12.4. Greenbelt, MD, USA: Goddard Space Flight Center Distributed Active Archive Center (GSFC DAAC). [https://doi.org/10.5067/QBZ6MG944HW0, Accessed 3/18/2019].

[dataset] Global Modeling and Assimilation Office (GMAO) (2015b). MERRA-2 Tavg1_2d_slv_Nx: 2d,1-Hourly, Time-Averaged, Single-Level, Assimilation, Single-Level Diagnostics V5.12.4. Greenbelt, MD, USA: Goddard Space Flight Center Distributed Active Archive Center (GSFC DAAC). [https://doi.org/10.5067/VJAFPLI1CSIV, Accessed 3/19/2019].

[dataset] Global Modeling and Assimilation Office (GMAO) (2015c). MERRA-2 Tavg1_2d_chm_Nx: 2d,1-Hourly, Time-Averaged, Single-Level, Assimilation, carbon Monoxide and Ozone Diagnostics V5.12.4. Greenbelt,

MD, USA: Goddard Space Flight Center Distributed Active Archive Center (GSFC DAAC). [https://doi.org/10.5067/3RQ5YS674DG, Accessed 3/21/2019].

Harnik, N., Chang, E.K.M., 2003. Storm Track Variations As Seen in Radiosonde Observations and Reanalysis Data. J. Clim. 16, 480–495. https://doi.org/10.1175/1520-0442(2003)016<0480:STVASI>2.0.CO;2

Herman, J., Cede, A., Spinei, E., Mount, G., Tzortziou, M., Abuhassan, N., 2009. NO_2 column amounts from ground-based Pandora and MFDOAS spectrometers using the direct-sun DOAS technique: Intercomparisons and application to OMI validation. J. Geophys. Res. 114, D13307. https://doi.org/10.1029/2009JD011848

Herman, J., Evans, R., Cede, A., Abuhassan, N., Petropavlovskikh, I., McConville, G., 2015. Comparison of ozone retrievals from the Pandora spectrometer system and Dobson spectrophotometer in Boulder, Colorado. Atmos. Meas. Tech. 8, 3407–3418. https://doi.org/10.5194/amt-8-3407-2015

Holton, J.R., Haynes, P.H., McIntyre, M.E., Douglass, A.R., Rood, R.B., Pfister, L., 1995. Stratosphere-troposphere exchange. Rev. Geophys. 33, 403. https://doi.org/10.1029/95RG02097

Jaeglé, L., Wood, R., Wargan, K., 2017. Multiyear Composite View of Ozone Enhancements and Stratosphere-to-Troposphere Transport in Dry Intrusions of Northern Hemisphere Extratropical Cyclones. J. Geophys. Res. Atmos. 122, 13,436-13,457. https://doi.org/10.1002/2017JD027656

Kaldunski, B., Pierce, B., Holloway, T., 2017. When Stratospheric Ozone Hits Ground-level Regulation: Exceptional Events in Wyoming. Bull. Am. Meteorol. Soc. 98, 889–892. https://doi.org/10.1175/BAMS-D-14-00133.1

Kerr, J.B., McElroy, C., Evans, W.F.J., 1984. The automated Brewer spectrophotometer, in: Zerefos, C.S., Ghazi, A. (Eds.), Proceedings of the Quadrennial Ozone Symposium. American Meteorological Society, Boston, Mass., pp. 396–401.

Knowland, K. E., Doherty, R.M., Hodges, K.I., 2015. The effects of springtime mid-latitude storms on trace gas composition determined from the MACC reanalysis. Atmos. Chem. Phys. 15, 3605–3628. https://doi.org/10.5194/acp-15-3605-2015

Knowland, K.E., Ott, L.E., Duncan, B.N., Wargan, K., 2017a. Stratospheric Intrusion-Influenced Ozone Air Quality Exceedances Investigated in the NASA MERRA-2 Reanalysis. Geophys. Res. Lett. 44, 10,691-10,701. https://doi.org/10.1002/2017GL074532

Knowland, K.E., Doherty, R.M., Hodges, K.I., Ott, L.E., 2017b. The influence of mid-latitude cyclones on European background surface ozone. Atmos. Chem. Phys. 17, 12421–12447. https://doi.org/10.5194/acp-17-12421-2017

Labow, G.J., McPeters, R.D., Bhartia, P.K., Kramarova, N., 2013. A comparison of 40 years of SBUV measurements of column ozone with data from the Dobson/Brewer network. J. Geophys. Res. Atmos. 118, 7370–7378. https://doi.org/10.1002/jgrd.50503

Lamarque, J.-F., Hess, P.G., 1994. Cross-Tropopause Mass Exchange and Potential Vorticity Budget in a Simulated Tropopause Folding. J. Atmos. Sci. 51, 2246–2269. https://doi.org/10.1175/1520-0469(1994)051<2246:CTMEAP>2.0.CO;2

Langford, A.O., 1999. Stratosphere-troposphere exchange at the subtropical jet: Contribution to the tropospheric ozone budget at midlatitudes. Geophys. Res. Lett. 26, 2449–2452. https://doi.org/10.1029/1999GL900556

Langford, A.O., Masters, C.D., Proffitt, M.H., Hsie, E.-Y., Tuck, A.F., 1996. Ozone measurements in a tropopause fold associated with a cut-off low system. Geophys. Res. Lett. 23, 2501–2504. https://doi.org/10.1029/96GL02227

Langford, A.O., Aikin, K.C., Eubank, C.S., Williams, E.J., 2009. Stratospheric contribution to high surface ozone in Colorado during springtime. Geophys. Res. Lett. 36, L12801. https://doi.org/10.1029/2009GL038367

Langford, A.O., Brioude, J., Cooper, O.R., Senff, C.J., Alvarez, R.J., Hardesty, R.M., Johnson, B.J., Oltmans, S.J., 2012. Stratospheric influence on surface ozone in the Los Angeles area during late spring and early summer of 2010. J. Geophys. Res. Atmos. 117. https://doi.org/10.1029/2011JD016766

Langford, A.O., Alvarez, R.J., Brioude, J., Evan, S., Iraci, L.T., Kirgis, G., Kuang, S., Leblanc, T., Newchurch, M.J., Pierce, R.B., Senff, C.J., Yates, E.L., 2017. Coordinated profiling of stratospheric intrusions and transported pollution by the Tropospheric Ozone Lidar Network (TOLNet) and NASA Alpha Jet experiment (AJAX): Observations and comparison to HYSPLIT, RAQMS, and FLEXPART. Atmos. Environ. 174, 1–14. https://doi.org/10.1016/j.atmosenv.2017.11.031

Lefohn, A.S., Wernli, H., Shadwick, D., Limbach, S., Oltmans, S.J., Shapiro, M., 2011. The importance of stratospheric-tropospheric transport in affecting surface ozone concentrations in the western and northern tier of the United States. Atmos. Environ. 45, 4845–4857. https://doi.org/10.1016/j.atmosenv.2011.06.014

Levelt, P.F., van den Oord, G.H.J., Dobber, M.R., Malkki, A., Huib Visser, Johan de Vries, Stammes, P., Lundell, J.O.V., Saari, H., 2006. The ozone monitoring instrument. IEEE Trans. Geosci. Remote Sens. 44, 1093–1101. https://doi.org/10.1109/TGRS.2006.872333

Lin, M., Fiore, A.M., Cooper, O.R., Horowitz, L.W., Langford, A.O., Ii, H.L., Johnson, B.J., Naik, V., Oltmans, S.J., Senff, C.J., 2012. Springtime high surface ozone events over the western United States : Quantifying the role of stratospheric intrusions 117, 1–20. https://doi.org/10.1029/2012JD018151

McCarty, W., Coy, L., Gelaro, R., Huang, A., Merkova, D., Smith, E.B., Sienkiewicz, M., Wargan, K., 2016. MERRA-2 input observations: Summary and assessment. NASA/TM–2016–104606 46, 64.

McClain, E.P., 1960. Some effects of the western Cordillera of North America of cyclonic activity. J. Meteorol. 17, 104–115. https://doi.org/10.1175/1520-0469(1960)017<0104:SEOTWC>2.0.CO;2

McPeters, R., Kroon, M., Labow, G., Brinksma, E., Balis, D., Petropavlovskikh, I., Veefkind, J.P., Bhartia, P.K., Levelt, P.F., 2008. Validation of the Aura Ozone Monitoring Instrument total column ozone product. J. Geophys. Res. 113, 1–9. https://doi.org/10.1029/2007jd008802

Monahan, K.P., Pan, L.L., McDonald, A.J., Bodeker, G.E., Wei, J., George, S.E., Barnet, C.D., Maddy, E., 2007. Validation of AIRS v4 ozone profiles in the UTLS using ozonesondes from Lauder, NZ and Boulder, USA. J. Geophys. Res. Atmos. 112, 1–11. https://doi.org/10.1029/2006JD008181

Monks, P.S., 2000. A review of the observations and origins of the spring ozone maximum. Atmos. Environ. 34, 3545–3561. https://doi.org/10.1016/S1352-2310(00)00129-1

Müller, M., Tiefengraber, M., & Cede, A. Jan. 2017. Report 2016011. ESA Ground-Based Air-Quality Spectrometer Validation Network and Uncertainties Study: Validation Reports. Luftblick Earth Observation Technologies. http://pandonia.net/media/documents/LuftBlick_Pandonia_Validation_RP_2016011_v2.0.pdf

Nowlan, C.R., Liu, X., Janz, S.J., Kowalewski, M.G., Chance, K., Follette-Cook, M.B., Fried, A., González Abad, G., Herman, J.R., Judd, L.M., Kwon, H.-A., Loughner, C.P., Pickering, K.E., Richter, D., Spinei, E., Walega, J., Weibring, P., Weinheimer, A.J., 2018. Nitrogen dioxide and formaldehyde measurements from the GEOstationary Coastal and Air Pollution Events (GEO-CAPE) Airborne Simulator over Houston, Texas. Atmos. Meas. Tech. 11, 5941–5964. https://doi.org/10.5194/amt-11-5941-2018

Olsen, M.A., Gallus, W.A., Stanford, J.L., Brown, J.M., 2000. Fine-scale comparison of TOMS total ozone data with model analysis of an intense Midwestern cyclone. J. Geophys. Res. Atmos. 105, 20487–20495. https://doi.org/10.1029/2000JD900205

Ott, L.E., Duncan, B.N., Thompson, A.M., Diskin, G., Fasnacht, Z., Langford, A.O., Lin, M., Molod, A.M., Nielsen, J.E., Pusede, S.E., Wargan, K., Weinheimer, A.J., Yoshida, Y., 2016. Frequency and impact of summertime stratospheric intrusions over Maryland during DISCOVER-AQ (2011): New evidence from NASA's GEOS-5 simulations. J. Geophys. Res. Atmos. 121, 3687–3706. https://doi.org/10.1002/2015JD024052

Platt, U., Stutz, J., 2008. Differential Optical Absorption Spectroscopy: Principles and Applications. Physics of Earth and Space Environments. Springer, Berlin.

Reed, A.J., Thompson, A.M., Kollonige, D.E., Martins, D.K., Tzortziou, M.A., Herman, J.R., Berkoff, T.A., Abuhassan, N.K., Cede, A., 2013. Effects of local meteorology and aerosols on ozone and nitrogen dioxide retrievals from OMI and pandora spectrometers in Maryland, USA during DISCOVER-AQ 2011. J. Atmos. Chem. 72, 455–482. https://doi.org/10.1007/s10874-013-9254-9

Ryoo, J.M., Yates, E.L., Iraci, L.T., Yates, E.L., Gore, W., 2017. Investigating sources of ozone over California using AJAX airborne measurements and models: Assessing the contribution from long-range transport. Atmos. Environ. 155, 53–67. https://doi.org/10.1016/j.atmosenv.2017.02.008

Shapiro, M.A., 1980. Turbulent Mixing within Tropopause Folds as a Mechanism for the Exchange of Chemical Constituents between the Stratosphere and Troposphere. J. Atmos. Sci. 37, 994–1004. https://doi.org/10.1175/1520-0469(1980)037<0994:TMWTFA>2.0.CO;2

Singh, H.B., Ludwig, F.L., Johnson, W.B., 1978. Tropospheric ozone: Concentrations and variabilities in clean remote atmospheres. Atmos. Environ. 12, 2185–2196. https://doi.org/10.1016/0004-6981(78)90174-9

Škerlak, B., Sprenger, M., Wernli, H., 2014. A global climatology of stratosphere–troposphere exchange using the ERA-Interim data set from 1979 to 2011. Atmos. Chem. Phys. 14, 913–937. https://doi.org/10.5194/acp-14-913-2014

Spinei, E., Whitehill, A., Fried, A., Tiefengraber, M., Knepp, T.N., Herndon, S., Herman, J.R., Müller, M., Abuhassan, N., Cede, A., Richter, D., Walega, J., Crawford, J., Szykman, J., Valin, L., Williams, D.J., Long, R., Swap, R.J., Lee, Y., Nowak, N., Poche, B., 2018. The first evaluation of formaldehyde column observations by improved Pandora spectrometers during the KORUS-AQ field study. Atmos. Meas. Tech. 11, 4943–4961. https://doi.org/10.5194/amt-11-4943-2018

Stohl, A., Spichtinger-Rakowsky, N., Bonasoni, P., Feldmann, H., Memmesheimer, M., Scheel, H.., Trickl, T., Hübener, S., Ringer, W., Mandl, M., 2000. The influence of stratospheric intrusions on alpine ozone concentrations. Atmos. Environ. 34, 1323–1354. https://doi.org/10.1016/S1352-2310(99)00320-9

Stohl, A., Bonasoni, P., Cristofanelli, P., Collins, W., Feichter, J., Frank, A., Forster, C., Gerasopoulos, E., Gäggeler, H., James, P., Kentarchos, T., Kromp-Kolb, H., Krüger, B., Land, C., Meloen, J., Papayannis, A., Priller, A., Seibert, P., Sprenger, M., Roelofs, G.J., Scheel, H.., Schnabel, C., Siegmund, P., Tobler, L., Trickl, T., Wernli, H., Wirth, V., Zanis, P., Zerefos, C., 2003. Stratosphere-troposphere exchange: A review, and what we have learned from STACCATO. J. Geophys. Res. 108, 8516. https://doi.org/10.1029/2002JD002490

Susskind, J., Barnet, C., Blaisdell, J., Iredell, L., Keita, F., Kouvaris, L., Molnar, G., Chahine, M., 2006. Accuracy of geophysical parameters derived from Atmospheric Infrared Sounder/Advanced Microwave Sounding Unit as a function of fractional cloud cover. J. Geophys. Res. 111, D09S17. https://doi.org/10.1029/2005JD006272

Susskind, J., Blaisdell, J.M., Iredell, L., 2014. Improved methodology for surface and atmospheric soundings, error estimates, and quality control procedures: the atmospheric infrared sounder science team version-6 retrieval algorithm. J. Appl. Remote Sens. 8, 084994. https://doi.org/10.1117/1.JRS.8.084994

Swap, R., Cede, A., Abuhassan, N., Tiefengraber, M., Szykman, J., Dehn, A., Von Bismarck, J., Lefer, B., Dec. 2018. From Research/Campaign Mode to Long-Term Air Quality Monitoring: The Evolution of the Pandonia Global Network (PGN). Paper presented at the 2018 American Geophysical Union Fall Meeting, Washington, D.C.

Tiefengraber, M., Cede, A., Jan. 2017. Report 2017002. ESA Ground-Based Air-Quality Spectrometer Validation Network and Uncertainties Study: Network Inter-comparison Campaign Report. Luftblick Earth Observation Technologies. http://pandonia.net/media/documents/LuftBlick_Pandonia_NetworkIntercomparison_RP_2017002_v1.0.pdf

Tzortziou, M., Herman, J.R., Cede, A., Abuhassan, N., 2012. High precision, absolute total column ozone measurements from the Pandora spectrometer system: Comparisons with data from a Brewer double monochromator and Aura OMI. J. Geophys. Res. Atmos. 117, 1–14. https://doi.org/10.1029/2012JD017814

Veefkind, J.P., Aben, I., McMullan, K., Förster, H., de Vries, J., Otter, G., Claas, J., Eskes, H.J., de Haan, J.F., Kleipool, Q., van Weele, M., Hasekamp, O., Hoogeveen, R., Landgraf, J., Snel, R., Tol, P., Ingmann, P., Voors, R., Kruizinga, B., Vink, R., Visser, H., Levelt, P.F., 2012. TROPOMI on the ESA Sentinel-5 Precursor: A GMES mission for global observations of the atmospheric composition for climate, air quality and ozone layer applications. Remote Sens. Environ. 120, 70–83. https://doi.org/10.1016/j.rse.2011.09.027

Verhoelst, T., Granville, J., Hendrick, F., Köhler, U., Lerot, C., Pommereau, J.-P., Redondas, A., Van Roozendael, M., Lambert, J.-C., 2015. Metrology of ground-based satellite validation: co-location mismatch and smoothing issues of total ozone comparisons. Atmos. Meas. Tech. 8, 5039–5062. https://doi.org/10.5194/amt-8-5039-2015

Wargan, K., Labow, G., Frith, S., Pawson, S., Livesey, N., Partyka, G., 2017. Evaluation of the Ozone Fields in NASA's MERRA-2 Reanalysis. J. Clim. 30, 2961–2988. https://doi.org/10.1175/JCLI-D-16-0699.1

Waters, J.W., Froidevaux, L., Harwood, R.S., Jarnot, R.F., Pickett, H.M., Read, W.G., Siegel, P.H., Cofield, R.E., Filipiak, M.J., Flower, D.A., Holden, J.R., Lau, G.K., Livesey, N.J., Manney, G.L., Pumphrey, H.C., Santee, M.L., Wu, D.L., Cuddy, D.T., Lay, R.R., Loo, M.S., Perun, V.S., Schwartz, M.J., Stek, P.C., Thurstans, R.P., Boyles, M.A., Chandra, K.M., Chavez, M.C., Gun-Shing Chen, Chudasama, B.V., Dodge, R., Fuller, R.A., Girard, M.A., Jiang, J.H., Yibo Jiang, Knosp, B.W., LaBelle, R.C., Lam, J.C., Lee, K.A., Miller, D., Oswald, J.E., Patel, N.C., Pukala, D.M., Quintero, O., Scaff, D.M., Van Snyder, W., Tope, M.C., Wagner, P.A., Walch, M.J., 2006. The Earth observing system microwave limb sounder (EOS MLS) on the aura Satellite. IEEE Trans. Geosci. Remote Sens. 44, 1075–1092. https://doi.org/10.1109/TGRS.2006.873771

Wirth, V., Egger, J., 1999. Diagnosing extratropical synoptic-scale stratosphere-troposphere exchange: A case study. Q. J. R. Meteorol. Soc. 125, 635–655. https://doi.org/10.1002/qj.49712555413

Young, M. V., Monk, G.A., Browning, K.A., 1987. Interpretation of Satellite Imagery of A Rapidly Deepening Cyclone. Q. J. R. Meteorol. Soc. 113, 1089–1115. https://doi.org/10.1002/qj.49711347803

Zoogman, P., Liu, X., Suleiman, R.M., Pennington, W.F., Flittner, D.E., Al-Saadi, J.A., Hilton, B.B., Nicks, D.K., Newchurch, M.J., Carr, J.L., Janz, S.J., Andraschko, M.R., Arola, A., Baker, B.D., Canova, B.P., Chan Miller, C., Cohen, R.C., Davis, J.E., Dussault, M.E., Edwards, D.P., Fishman, J., Ghulam, A., González Abad, G., Grutter, M., Herman, J.R., Houck, J., Jacob, D.J., Joiner, J., Kerridge, B.J., Kim, J., Krotkov, N.A., Lamsal, L., Li, C., Lindfors, A., Martin, R.V., McElroy, C.T., McLinden, C., Natraj, V., Neil, D.O., Nowlan, C.R., O'Sullivan, E.J., Palmer, P.I., Pierce, R.B., Pippin, M.R., Saiz-Lopez, A., Spurr, R.J.D., Szykman, J.J., Torres, O., Veefkind, J.P., Veihelmann, B., Wang, H., Wang, J., Chance, K., 2017. Tropospheric emissions: Monitoring of pollution (TEMPO). J. Quant. Spectrosc. Radiat. Transf. 186, 17–39. https://doi.org/10.1016/j.jqsrt.2016.05.008